SCIENCE CHINA Materials LETTERS

mater.scichina.com link.springer.com

Published online 27 July 2021 | https://doi.org/10.1007/s40843-021-1719-8
Sci China Mater 2021, 64(12): 3131–3137

Strengthening mechanisms of high-performance Al-Mn-Mg-Sc-Zr alloy fabricated by selective laser melting

Yaoxiang Geng[1*], Hao Tang[1], Junhua Xu[1*], Zhijie Zhang[1], Yakai Xiao[2] and Yi Wu[2]

Selective laser melting (SLM) can efficiently fabricate metallic components with complex shapes and offers new opportunities for the structural optimization of lightweight components [1]. Owing to the high cooling rate (10^3–10^6 K s^{-1}) of the SLM process, the solidified SLM-fabricated metals show a unique microstructure with highly supersaturated solid solutions that are well beyond the normal solubility limits of most elements. This leads to significant improvements in the mechanical properties of the SLM-fabricated materials [2].

Although the SLM technology has been used to fabricate many different types of metallic materials [3], the use of SLM for aluminum powders is challenging due to their high laser reflectivity, persistent surface oxidation, poor spreadability, and high thermal conductivity [4]. Therefore, most of the SLM aluminum alloys are currently still based on the near eutectic Al-Si casting alloys. Unfortunately, the yield strength (YS) and ultimate tensile strength (UTS) of these alloys are no greater than 300 and 500 MPa, respectively [5]. Recently, Geng *et al.* [6,7] reported a high-strength AlSiMg1.4 alloy specifically designed for SLM. The alloy exhibited a relatively high YS of 341 ± 14 MPa and a high UTS of 518 ± 6 MPa, along with a total elongation of 7.1% ± 0.4%. However, the strength of these alloys is still much lower than that of the traditional high-strength aluminum alloys (e.g., 7xxx) [8]. While many attempts have been made to manufacture high-performance 2xxx, 6xxx, and 7xxx alloys, the obtained alloys show pronounced cracking and pore formation during the SLM process due to their high concentrations of alloying elements and wide solidification ranges [9]. The inoculants (e.g., Si, Zr, and Ti) introduced into these alloys can act as nucleation sites for α-Al crystallization, and favor the formation of fine grains to avoid the appearance of solidification cracks [10–13]. However, the mechanical properties of such doped alloys are still far lower than those of their wrought counterparts.

The addition of Sc and Zr to the 5xxx series (Al-Mg) alloys is of particular interest for high-performance structural applications due to the high strength, excellent fatigue resistance, and creep resistance of these alloys [14]. Scalmalloy® (Al-4.5Mg-0.66Sc-0.37Zr, wt.%) was specifically designed for SLM by increasing the content of Sc and Zr from those of the traditional Sc- and Zr-modified Al-Mg aluminum alloys [15]. The alloy exhibits a very fine equiaxed-columnar bimodal grain structure and shows high strength and ductility with YS, UTS, and elongation of 520, 530 MPa, and 14%, respectively [15,16]. Recently, Li *et al.* [17] designed a new Si-containing Al-8.0Mg-1.3Si-0.5Mn-0.5Sc-0.3Zr alloy. The results showed that this SLM alloy demonstrated a significantly refined microstructure. After the aging treatment, the maximum UTS of the alloy reached to 550 MPa. Ma *et al.* [18] investigated the effect of cold rolling on the microstructure and properties of the SLM Al-Mg-Sc-Zr alloy. After cold rolling, the microstructure of the alloy was refined and the alloy strength was enhanced, but its plasticity showed a clear decrease. To ameliorate the inherent corrosion sensitivity and laser incompatibility of Al-Mg alloys, Jia *et al.* [19] designed a high-strength SLM Al-Mn-Sc alloy. The new alloy showed a YS of up to 560 MPa and ductility of approximately 18% after appropriate heat treatment. For the Sc- and Zr-modified aluminum alloys, the formation of fine equiaxed grains can facilitate improved liquid feeding and the accommodation of strains generated during the rapid solidification process to avoid hot-tearing cracks, result-

[1] School of Materials Science and Engineering, Jiangsu University of Science and Technology, Zhenjiang 212003, China
[2] State Key Laboratory of Metal Matrix Composites, Shanghai Jiao Tong University, Shanghai 200240, China
* Corresponding authors (emails: yaoxianggeng@163.com (Geng Y); jhxu@just.edu.cn (Xu J))

ing in good processability [19]. The improvement of the strength of the alloys is mainly attributed to the reduced grain size, high concentration of the solid solution elements, and precipitation of the high-density Al_3Sc nanoparticles [20]. To date, the strengths of the SLM aluminum alloys have been found to be lower than 600 MPa. It is necessary to further improve their strength to meet the high requirements of industrial applications.

In this study, a new Al-Mn-Mg-Sc-Zr alloy specifically designed for SLM was obtained by increasing the (Mn +Mg) and (Sc+Zr) contents based on the rapid solidification characteristics of the SLM process. The alloy exhibits good processability with a maximum relative density approaching 100% and excellent mechanical properties with YS, UTS, and elongation range of 547–620 MPa, 578–647 MPa, and 2.3%–9.8%, respectively.

The raw material powder of Al-Mn-Mg-Sc-Zr (d_{10}: 21.65 μm, d_{50}: 38.81 μm, d_{90}: 61.99 μm) was prepared by a vacuum induction N_2 gas atomisation (VIGA) process. The particle size distribution was characterized by using a Bettersize 3000 laser particle size tester. The powder has a chemical composition of Al-5.50Mn-2.69Mg-1.03Sc-0.91Zr-0.10Fe (in wt.%), as tested by an inductively coupled plasma atomic scanning spectrometer (ICP, PE OPTIMA 7300DV). The SLM specimens with a size of 50 mm × 15 mm × 15 mm were fabricated using EP-M250 equipment with a spot size of 100 μm on the building area. The SLM process parameters used were: laser power of 250 and 350 W, layer thickness of 30 μm, hatch spacing of 100 μm, and scanning speed of 800–1200 mm s^{-1}. The direction of scanning was rotated at 67° between consecutive layers. Before starting the SLM process, the building platform was heated to 200°C. The specimens for the tensile test were produced in accordance with a laser power of 350 W and a scanning speed of 800 mm s^{-1}.

The microstructure of the sample was analyzed with an optical microscope (OM, Axio Vert.A1) and a scanning electron microscope (SEM, JSM-6480, at 200 kV). The transmission electron microscopy (TEM) investigations were performed on a JEM-2010 F with an energy dispersive X-ray spectroscopy (EDXS) attachment. Phase characterization was conducted by X-ray diffraction (XRD, Bruker D8 Focus, Cu-Kα radiation, λ = 0.15406 nm). The density of the SLM specimens was measured using the Archimedes method. To calculate the relative density, the theoretical density of this alloy in the as-cast state, which is 2.813 g cm^{-3}, was used. For the tensile tests of the as-fabricated and heat-treated specimens, a Zwick/Roell Z100 type universal testing machine was used at a constant strain rate of 1 mm min^{-1} according to the ASTM E8-04 standard. The data were the average values of three specimens.

Fig. 1a shows the relative density of the SLM samples obtained at different laser powers and scanning speeds. It is observed from Fig. 1a that the relative density decreases with increasing scanning speed under a fixed laser power. The samples fabricated at 350 W show a higher relative density than those fabricated at 250 W. The highest relative density of 99.82% is achieved at the laser power of 350 W and scanning speed of 800 mm s^{-1}, demonstrating the good processability of this alloy. All of the samples are crack-free. A typical layered build microstructure comprised by the accumulation of large weld lines in the cross-section is observed in the as-fabricated sample (the inset in Fig. 1a) [14]. As shown in Fig. 1b, some blocky Al_3(Sc,Zr) phases identified by EDXS can be observed in the SEM image of the as-fabricated sample, indicating the content of Sc and Zr exceeds the solubility in the present alloy. XRD patterns show the presence of the α-Al and Al_6Mn phases. No significant differences are observed between the as-fabricated and aged samples (Fig. 1c). TEM bright field image shows that the microstructure of the as-fabricated sample can be divided into two regions: the fine equiaxed grains with an average size of approximately 500 nm and the elongated columnar grains with an average length of approximately 3 μm (Fig. 1d). The high-resolution TEM (HRTEM) image and selected area electron diffraction (SAED) pattern obtained from the columnar grains show a uniform face-centered cubic (fcc) α-Al structure without Guinier Preston (GP) zones and precipitation (Fig. 1e). Fig. 2 shows the EDX maps of the as-fabricated sample. The Al-Mn-rich particles are mainly segregated along both equiaxed and columnar grain boundaries. According to the reports by Vlach *et al.* [21,22], these particles can be identified as Al_6Mn and/or Al_6(Mn,Fe) phases, which needs to be further clarified. The Al_3(Sc,Zr) particles are mainly located within the equiaxed grain regions [20].

The high Mn, Sc, and Zr concentrations achieved in the present Al-Mn-Mg-Sc-Z alloys exert several beneficial effects and play a key role in obtaining the desired high mechanical performance of the alloy. Upon rapid solidification, the primary Al_3(Sc,Zr) particles serve as nuclei for α-Al grains and achieve a strong grain refining effect, effectively improving the processability of the alloy [23]. Fine grains with a random orientation that are nucleated by primary precipitates are evident at the edge of the melt pool. As the remaining melt solidifies, the concentration

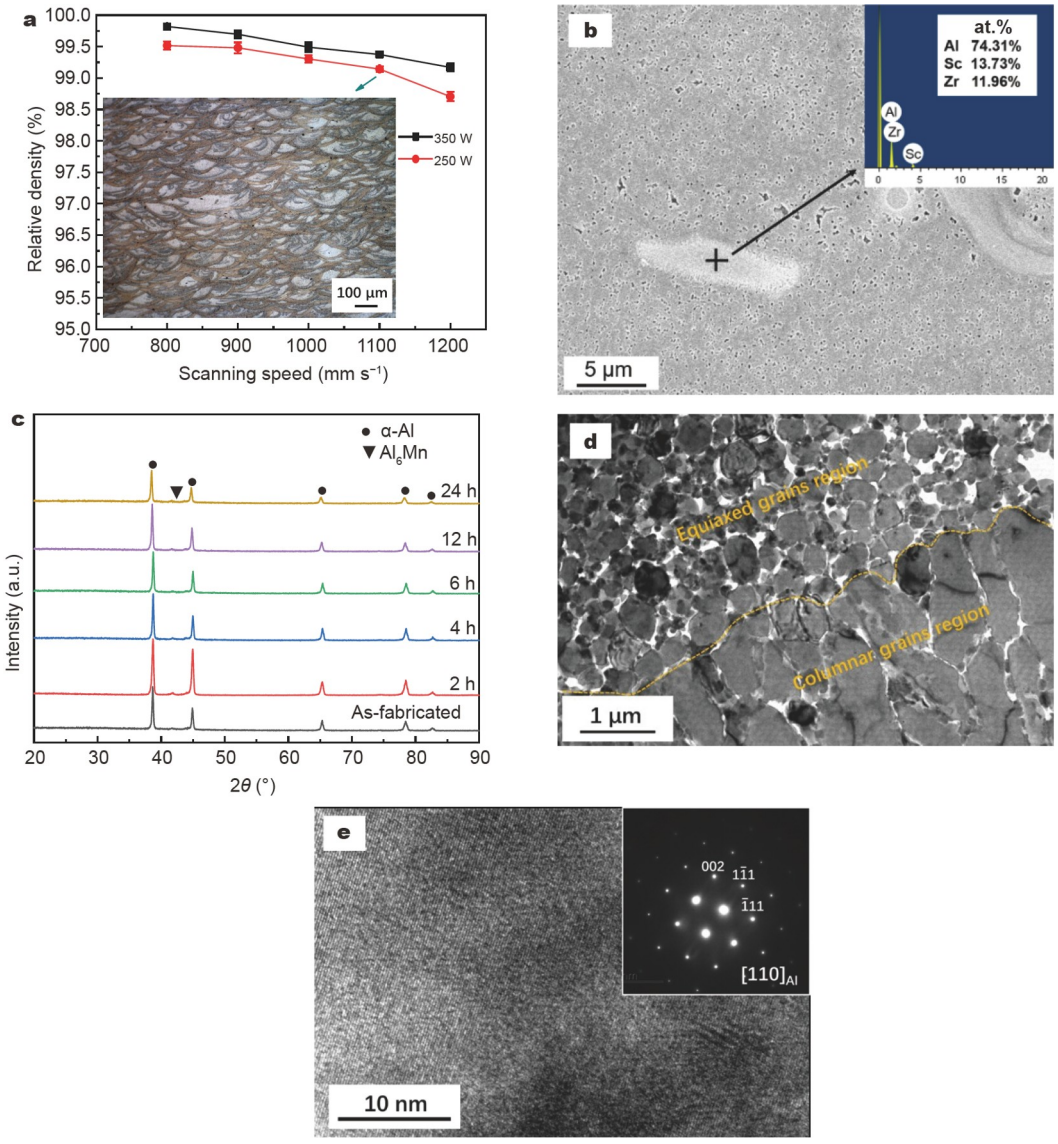

Figure 1 (a) Relative density as a function of laser scanning speed at the laser powers of 250 and 350 W, respectively (the inset shows the OM image of the sample fabricated at the laser power of 250 W and scanning speed of 1100 mm s^{-1}); (b) SEM image and EDS analysis of the as-fabricated sample; (c) XRD patterns of the as-fabricated samples and the samples after being aged at 300°C for different times; (d) TEM bright-field image of the as-fabricated sample, and the corresponding (e) HRTEM image and SAED pattern (inset) obtained from the columnar grains.

of Sc and Zr decreased continuously, and in the absence of the formation of Al_3(Sc,Zr) particles, coarse grains are nucleated by the underlying fine grains due to the decrease in the nucleation site density (Fig. 2b) [24].

Fig. 3 shows the TEM results for the as-fabricated samples after being aged at 300°C for 2 h. No significant changes can be observed from the TEM bright-field images. The alloy maintains the columnar-equiaxed bimodal microstructure with no obvious recrystallization or grain coarsening (Fig. 3a and b). The high thermal stability of the grain structure for the present alloy is attributed mainly to the thermally stable Al_6Mn and Al_3(Sc,Zr) particles that act as strong grain growth inhibitors to prevent recrystallization and grain growth [20]. However, the HRTEM images and the corresponding SAED patterns obtained from aged samples show that a large number of spherical nanoparticles (~2–5 nm) precipitate from the inside of both the equiaxed and columnar grains. These nanoparticles have the $L1_2$ structure shape that maintains a high coherency with the Al matrix

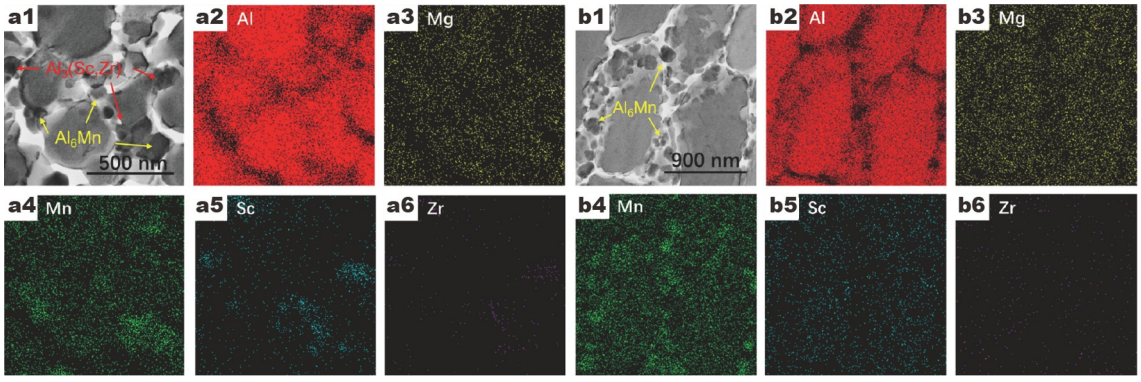

Figure 2 EDX mapping of the main elements (Al, Mg, Mn, Sc, and Zr) obtained from the (a) equiaxed and (b) columnar grain regions of the as-fabricated sample.

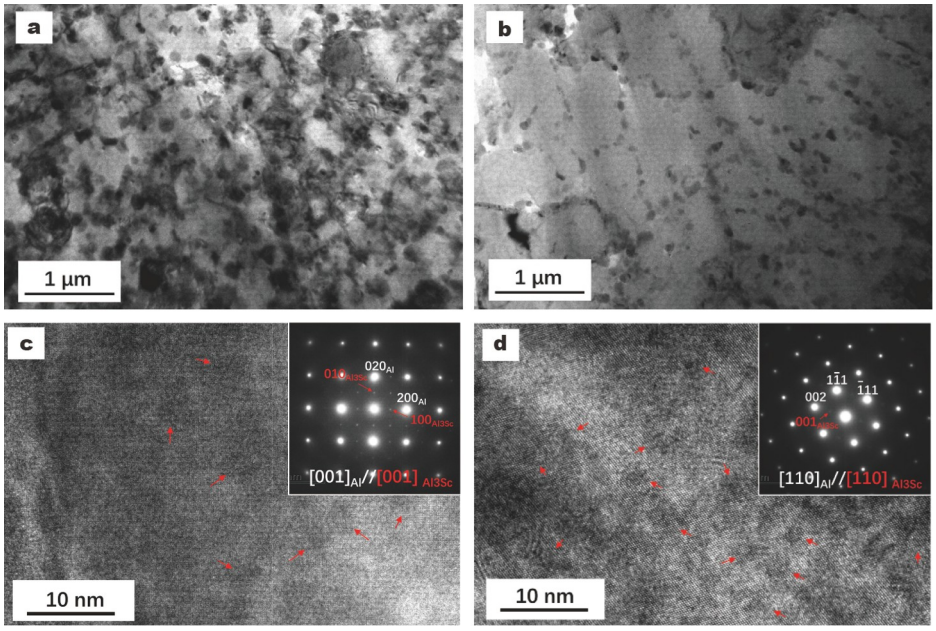

Figure 3 (a, b) TEM bright-field images, and (c, d) HRTEM images for the samples after being aged at 300°C for 2 h. (a) and (c) obtained from an equiaxed grain, and (b) and (d) obtained from a columnar grain. The insets in (c) and (d) show the SAED patterns.

(Fig. 3c and d) and are assigned to the secondary Al_3Sc phase [19].

Fig. 4 shows the results obtained for the mechanical properties of the SLM Al-Mn-Mg-Sc-Zr samples at different conditions and a comparison of the mechanical properties of this alloy to other SLM and traditional aluminum alloys. For the as-fabricated samples, the YS and UTS are 547 ± 3 MPa and 578 ± 2 MPa, respectively, with an elongation of 9.8% ± 0.1% (Fig. 4a and b). After being aged at 300°C for 2 h, the YS and UTS increased significantly to 616 ± 7 MPa and 637 ± 8 MPa, respectively, and the elongation decreased to 5.7% ± 0.9%. With a further increase in the aging time, the strength of the samples first decreased slightly and then increased to the maximum value at 24 h (YS = 621 ± 7 MPa and UTS = 647 ± 9 MPa). These values are superior to the YS and UTS values of most previously reported SLM-fabricated and wrought 7xxx aluminum alloys (Fig. 4c, d) [4,5,7,8,15–17,19,20,25–31].

The main strengthening mechanisms that contribute to the high strength of the SLM Al-Mn-Mg-Sc-Zr alloy arise from grain boundary strengthening, solid solution strengthening (mainly from the Mn, Mg, and Zr solutes), and precipitation hardening (mainly from the Al_3Sc

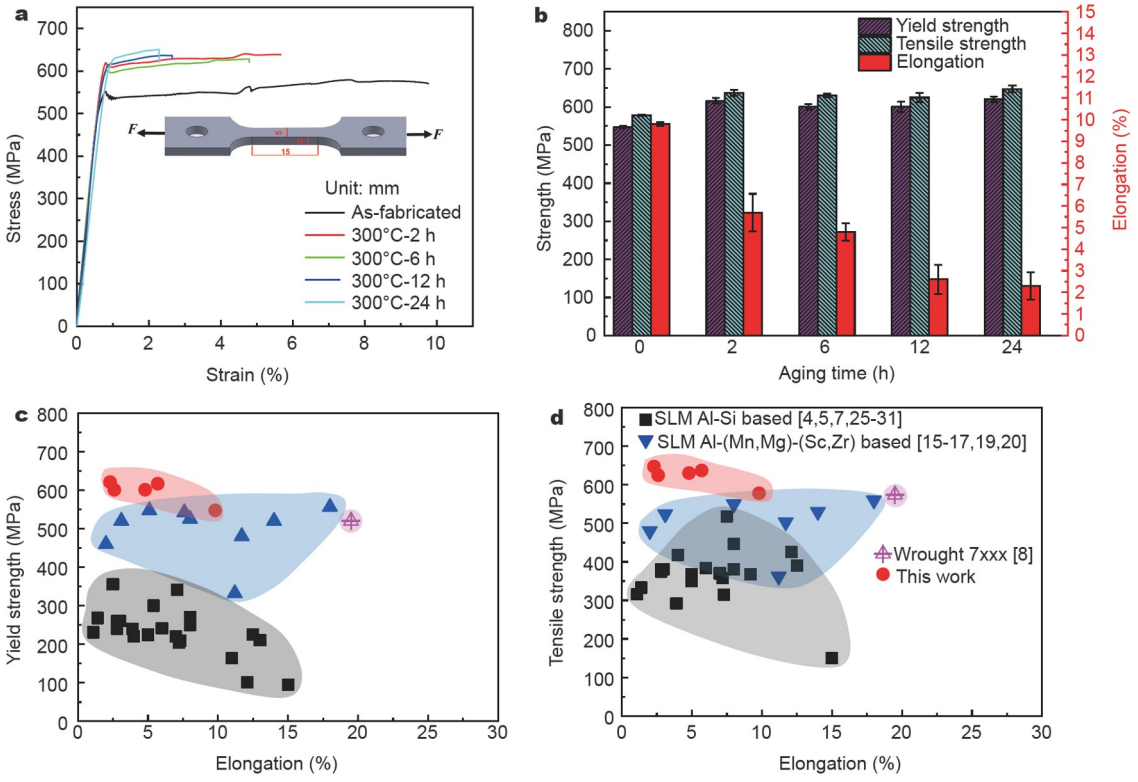

Figure 4 (a) Typical engineering stress-strain curves of the developed SLM Al-Mn-Mg-Sc-Zr alloys before and after direct aging at 300°C for different times. (b) The corresponding YS, UTS, and ductility data. The corresponding (c) YS and (d) UTS of our alloy compared to those of known typical SLM and wrought 7xxx aluminum alloys.

precipitates). Owing to the effect of the high cooling rate of the SLM process, solid solutions with high concentrations of the Mn, Mg, Sc, and Zr alloying elements in α-Al are obtained. Such high concentrations of the Mn, Mg, Sc, and Zr solutes increase the local lattice strain field induced by the solid solution, thereby hindering the motion of dislocations and strengthening the as-fabricated alloy [32]. Upon the application of an aging treatment at 300°C to the as-fabricated alloy, the decomposition of the supersaturated Sc in solution gives rise to a high density of nano-sized Al_3Sc precipitates. These highly coherent Al_3Sc nanoparticles effectively impede the motion of dislocations due to the bulk modulus differences between the precipitates and the surrounding Al matrix, providing an additional significant increase in the alloy strength [21,33,34]. In addition, the obtained grain sizes of the present alloys are estimated to be approximately several to dozens of times finer than those of the grains in the comparable Al-Mg-Sc-Zr casting alloys, providing a partial explanation for the high strength of the alloys according to the classical Hall-Petch relationship [20,35]. For the alloy after the aging treatment at 300°C for a long time, the ultra-high-density Al_3Sc particles produce strong dislocation entanglement under the condition of stress concentration during the tensile process, which leads to the cracking of particles and the generation of micro-cracks [36,37]. These micro-cracks propagate rapidly and eventually lead to fracture of the alloy, and result in the decreasing elongation of the alloy [38,39].

In this work, an Al-Mn-Mg-Sc-Zr alloy with high (Mg+Mn) and (Sc+Zr) contents was designed to exploit the rapid solidification of the SLM process. The microstructure, mechanical properties, and strengthening mechanism of the Al-Mn-Mg-Sc-Zr alloy obtained by SLM were studied systematically. The alloy exhibits good SLM compatibility with a maximum relative density of 99.82%. The microstructure of the alloy is composed of fine equiaxed grains and coarse columnar grains. The Al_6Mn and $Al_3(Sc,Zr)$ particles are mainly segregated along the grain boundaries and the equiaxed grain regions, respectively. High YS and UTS of 547 ± 3 MPa and 578 ± 2 MPa with an elongation of 9.8% ± 0.1% are achieved for the as-fabricated alloy due to very fine grain size and the

formation of a solid solution with a high concentration of the alloying elements. After the aging treatment at 300°C, the precipitation of a high density of coherent nanosized Al_3Sc particles leads to a remarkable improvement in the mechanical properties of the alloys. Both YS and UTS for the aged alloys are greater than 600 MPa, with the elongation ranging from 2.3% to 5.7%. This novel SLM-fabricated alloy has broad application prospects in the industry due to its combination of good laser processability and excellent mechanical properties.

Received 22 March 2021; accepted 28 May 2021; published online 27 July 2021

1 Gu DD, Meiners W, Wissenbach K, *et al.* Laser additive manufacturing of metallic components: Materials, processes and mechanisms. Int Mater Rev, 2012, 57: 133–164
2 Shi Y, Yang K, Kairy SK, *et al.* Effect of platform temperature on the porosity, microstructure and mechanical properties of an Al-Mg-Sc-Zr alloy fabricated by selective laser melting. Mater Sci Eng-A, 2018, 732: 41–52
3 Li N, Huang S, Zhang G, *et al.* Progress in additive manufacturing on new materials: A review. J Mater Sci Tech, 2019, 35: 242–269
4 Wang XJ, Zhang LC, Fang MH, *et al.* The effect of atmosphere on the structure and properties of a selective laser melted Al-12Si alloy. Mater Sci Eng-A, 2014, 597: 370–375
5 Aboulkhair NT, Simonelli M, Parry L, *et al.* 3D printing of aluminium alloys: Additive manufacturing of aluminium alloys using selective laser melting. Prog Mater Sci, 2019, 106: 100578
6 Geng YX, Fan SM, Jian JL, *et al.* Mechanical properties of AlSiMg alloy specifically designed for selective laser melting. Acta Metall Sin, 2020, 56: 821–830
7 Geng Y, Wang Y, Xu J, *et al.* A high-strength AlSiMg1.4 alloy fabricated by selective laser melting. J Alloys Compd, 2021, 867: 159103
8 Liao Y, Han X, Zeng M, *et al.* Influence of Cu on microstructure and tensile properties of 7XXX series aluminum alloy. Mater Des, 2015, 66: 581–586
9 Zhang J, Song B, Wei Q, *et al.* A review of selective laser melting of aluminum alloys: Processing, microstructure, property and developing trends. J Mater Sci Tech, 2019, 35: 270–284
10 Zhang H, Zhu H, Qi T, *et al.* Selective laser melting of high strength Al-Cu-Mg alloys: Processing, microstructure and mechanical properties. Mater Sci Eng-A, 2016, 656: 47–54
11 Martin JH, Yahata BD, Hundley JM, *et al.* 3D printing of high-strength aluminium alloys. Nature, 2017, 549: 365–369
12 Li L, Li R, Yuan T, *et al.* Microstructures and mechanical properties of Si and Zr modified Al-Zn-Mg-Cu alloy-A comparison between selective laser melting and spark plasma sintering. J Alloys Compd, 2020, 821: 153520
13 Tan Q, Zhang J, Sun Q, *et al.* Inoculation treatment of an additively manufactured 2024 aluminium alloy with titanium nanoparticles. Acta Mater, 2020, 196: 1–16
14 Li R, Wang M, Yuan T, *et al.* Selective laser melting of a novel Sc and Zr modified Al-6.2 Mg alloy: Processing, microstructure, and properties. Powder Tech, 2017, 319: 117–128
15 Schmidtke K, Palm F, Hawkins A, *et al.* Process and mechanical properties: Applicability of a scandium modified Al-alloy for laser additive manufacturing. Phys Procedia, 2011, 12: 369–374
16 Spierings AB, Dawson K, Uggowitzer PJ, *et al.* Influence of SLM scan-speed on microstructure, precipitation of Al_3Sc particles and mechanical properties in Sc- and Zr-modified Al-Mg alloys. Mater Des, 2018, 140: 134–143
17 Li R, Wang M, Li Z, *et al.* Developing a high-strength Al-Mg-Si-Sc-Zr alloy for selective laser melting: Crack-inhibiting and multiple strengthening mechanisms. Acta Mater, 2020, 193: 83–98
18 Ma R, Peng C, Cai Z, *et al.* Enhanced strength of the selective laser melted Al-Mg-Sc-Zr alloy by cold rolling. Mater Sci Eng-A, 2020, 775: 138975
19 Jia Q, Rometsch P, Kürnsteiner P, *et al.* Selective laser melting of a high strength Al Mn Sc alloy: Alloy design and strengthening mechanisms. Acta Mater, 2019, 171: 108–118
20 Jia Q, Zhang F, Rometsch P, *et al.* Precipitation kinetics, microstructure evolution and mechanical behavior of a developed Al-Mn-Sc alloy fabricated by selective laser melting. Acta Mater, 2020, 193: 239–251
21 Vlach M, Stulíková I, Smola B, *et al.* Annealing effects in hot-deformed Al-Mn-Sc-Zr alloys. Kovove Mater, 2015, 53: 295–304
22 Vlach M, Stulíková I, Smola B, *et al.* Precipitation in cold-rolled Al-Sc-Zr and Al-Mn-Sc-Zr alloys prepared by powder metallurgy. Mater Charact, 2013, 86: 59–68
23 Croteau JR, Griffiths S, Rossell MD, *et al.* Microstructure and mechanical properties of Al-Mg-Zr alloys processed by selective laser melting. Acta Mater, 2018, 153: 35–44
24 Kurz W, Trivedi R. Rapid solidification processing and microstructure formation. Mater Sci Eng-A, 1994, 179-180: 46–51
25 Bai Y, Yang Y, Xiao Z, *et al.* Process optimization and mechanical property evolution of AlSiMg0.75 by selective laser melting. Mater Des, 2018, 140: 257–266
26 Prashanth KG, Scudino S, Klauss HJ, *et al.* Microstructure and mechanical properties of Al-12Si produced by selective laser melting: Effect of heat treatment. Mater Sci Eng-A, 2014, 590: 153–160
27 Kimura T, Nakamoto T, Ozaki T, *et al.* Microstructural formation and characterization mechanisms of selective laser melted Al-Si-Mg alloys with increasing magnesium content. Mater Sci Eng-A, 2019, 754: 786–798
28 Wang M, Song B, Wei Q, *et al.* Effects of annealing on the microstructure and mechanical properties of selective laser melted AlSi7Mg alloy. Mater Sci Eng-A, 2019, 739: 463–472
29 Kimura T, Nakamoto T. Microstructures and mechanical properties of A356 (AlSi7Mg0.3) aluminum alloy fabricated by selective laser melting. Mater Des, 2016, 89: 1294–1301
30 Uzan NE, Shneck R, Yeheskel O, *et al.* High-temperature mechanical properties of AlSi10Mg specimens fabricated by additive manufacturing using selective laser melting technologies (AM-SLM). Addit Manuf, 2018, 24: 257–263
31 Xiong ZH, Liu SL, Li SF, *et al.* Role of melt pool boundary condition in determining the mechanical properties of selective laser melting AlSi10Mg alloy. Mater Sci Eng-A, 2019, 740-741: 148–156
32 Varvenne C, Leyson GPM, Ghazisaeidi M, *et al.* Solute strengthening in random alloys. Acta Mater, 2017, 124: 660–683
33 Ardell AJ. Precipitation hardening. Metall Trans A, 1985, 16: 2131–2165
34 Wang Q, Li Z, Pang S, *et al.* Coherent precipitation and strengthening in compositionally complex alloys: A review. Entropy, 2018, 20: 878
35 Hu J, Shi YN, Sauvage X, *et al.* Grain boundary stability governs

hardening and softening in extremely fine nanograined metals. Science, 2017, 355: 1292–1296
36 Ooi SW, Hill P, Rawson M, *et al.* Effect of retained austenite and high temperature Laves phase on the work hardening of an experimental maraging steel. Mater Sci Eng-A, 2013, 564: 485–492
37 Sun Q, Wang X, Zhang S, *et al.* Effect of microstructure on fracture toughness of new type hot-rolled nano-scale precipitation strengthening steel. Acta Metall Sin, 2013, 49: 1501–1507
38 Wu ZG, Song M, He YH. Effects of Er on the microstructure and mechanical properties of an as-extruded Al-Mg alloy. Mater Sci Eng-A, 2009, 504: 183–187
39 Lv ZP, Jiang SH, He JY, *et al.* Second phase strengthening in advance materl materials. Acta Metall Sin, 2016, 52: 1183–1198

Acknowledgements This work was supported by the National Natural Science Foundation of China (51801079 and 52001140), and the Natural Science Foundation for Young Scientists of Jiangsu, China (BK20180985 and BK20180987).

Author contributions Geng Y and Xu J conceived the idea and wrote the paper. Tang H and Zhang Z performed the experiments. Xiao Y and Wu Y conducted the tensile testing. All authors contributed to the general discussion.

Conflict of interest The authors declare that they have no conflict of interest.

Yaoxiang Geng is an associate professor at the School of Materials Science and Engineering, Jiangsu University of Science and Technology (China). He received his PhD degree in materials science (2016) from the School of Materials Science and Engineering, Dalian University of Technology (DUT). His research focuses on composition design and properties investigation of special aluminum alloys for selective laser melting and amorphous and nanocrystalline alloys.

Junhua Xu is a professor of the School of Materials Science and Engineering, Jiangsu University of Science and Technology (China). He received his PhD degree in materials science (2000) from the School of Materials Science and Engineering, Shanghai Jiao Tong University. His research focuses on thin film technologies and application of materials, composition design and property investigation of special aluminum alloys for selective laser melting.

选区激光熔化成形高性能Al-Mn-Mg-Sc-Zr合金的时效强化机理

耿遥祥[1*], 唐浩[1], 许俊华[1*], 张志杰[1], 肖亚开[2], 吴一[2]

摘要 针对当前应用选区激光熔化(SLM)成形铝合金强度较低的缺点，本研究基于SLM技术熔体快速冷却的技术特性，通过提升Al-Mn-Mg-Sc-Zr合金中合金化元素的含量，设计高(Mg+Mn)和高(Sc+Zr)含量的SLM专用铝合金，系统研究了合金的SLM成形性及时效处理对合金组织和力学性能的影响. 结果表明，新合金具有优异的SLM成形性，最大相对致密度可达99.82%. SLM成形合金具有细小等轴晶-柱状晶双峰结构. 等轴晶晶界处有Al_6Mn和$Al_3(Sc,Zr)$纳米颗粒析出，而柱状晶晶界处只存在Al_6Mn纳米颗粒，这些高稳定性纳米颗粒可有效抑制合金在时效处理过程中的回复再结晶. 经300°C时效处理后，样品的力学性能获得较大程度的提升，其屈服强度和抗拉强度均超过600 MPa，是现有已报道SLM成形铝合金的最高值，并且保持较好的延伸率. 细晶强化、固溶强化和Al_3Sc纳米颗粒析出强化的共同作用，是Al-Mn-Mg-Sc-Zr合金具有高强度的主要原因.

